Chapter

Perspective Chapter: An Overview of Titanium Dioxide, Uses, Applications and DFT Study of the Optoelectronic Properties of TiO_2 Brookite Clusters

Ife Elegbeleye, Edwin Mapasha, Eric Maluta and Regina Maphanga

Abstract

Titanium dioxide (TiO_2) also known as titania belongs to the class of transitions metal oxides. Titanium dioxide has become a metal oxide of fascinating significance in the research sphere due to its numerous environmental and industrial applications. This chapter presents an overview of the physical, crystal, structural and semiconductor properties of TiO_2 while delving into direct and indirect band gaps, fermi levels in semiconductors, density of states and carrier concentration. The environmental, pharmaceutical, deodorization, photovoltaic and water purification applications of TiO_2 were also discussed. Although TiO_2 clusters have become the focus of several computational studies, typical hardware has a higher processing power, giving way for the simulations of cumbersome systems, some cluster sizes used for some studies are relatively small and are not fit to handle specific problems or complex systems significant for photovoltaic applications. First-principle density functional theory calculation using computational software and GPAW that implements electron density represented on real space grids and the projector-augmented wave method were utilized in this study to investigate the optical and electronic characteristics of TiO_2 brookite clusters. The results of computational investigations on the optical and electrical characteristics of different-sized TiO_2 clusters and intricate systems for the purpose of simulating charge transfer mechanisms in hybrid organic-inorganic photovoltaics and photocatalytic obliteration of contaminants were presented in this chapter.

Keywords: titanium dioxide, photocatalysis, pharmaceutical applications, TiO_2 clusters, density functional theory

1. Introduction

Titanium dioxide (TiO_2), also known as titania, is a member of the transition metal oxides family [1]. Due to its application in pigments, demonstrated capacity as a

photocatalyst, and ability to support significant reactions, which are beneficial to the environment, like the production of hydrogen through water splitting, contaminated air and water treatment, and semiconductor material in dye-sensitized solar cells (DSSCs), TiO_2 has attracted increasing attention [2, 3–5]. It has also been extensively utilized in the fields of medicine, environmental protection, and renewable energy [6].

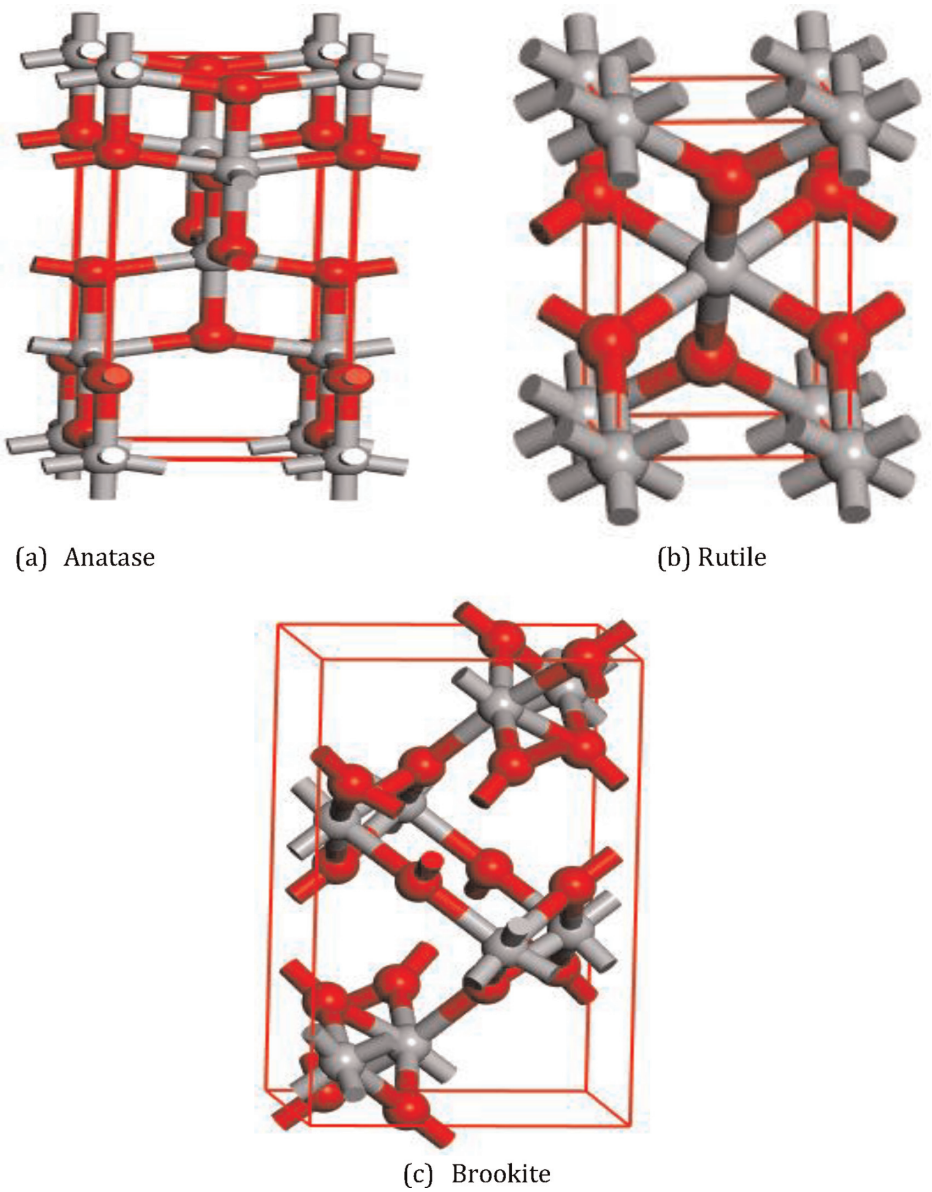

Figure 1.
Crystallographic forms of TiO_2 (a) anatase (b) rutile, and (c) brookite. The color scheme used throughout the study designates the atoms: red balls indicate oxygen atoms and gray balls indicate titanium atoms.

1.1 Polymorphs of TiO_2

Figure 1 shows the well-known polymorphs of TiO_2 structural models. The structures of the three TiO_2 polymorphs were imported from Dassault Systèmes BIOVIA Material Studio Accerlrys Inc. [7]. The structures of anatase, rutile, and brookite presented in **Figure 1** describe titanium atoms bonded by six oxygen atoms in a distorted octahedral configuration. While brookite crystalline structure is basically orthorhombic with each orthorhombic cell comprising eight formula unit. Anatase and rutile building blocks consist of a titanium atom surrounded by six oxygen atoms arranged in an octahedral that is distorted. The octahedral in the rutile phase forms chains that share vertices in the ab-plane and edges along the c-direction, while in the anatase structure, each octahedron shares four edges and forms zigzag chains along the a- and b-directions [1, 3, 8]. The two bonds between the octahedron of the oxygen and titanium atoms are slightly longer in each structure.

2. Applications of titanium dioxide

Titanium dioxide has so many applications ranging from deodorization, air purification, and photocatalysis, as shown in **Figure 2**.

2.1 Environmental improvement applications

Due to the nontoxic nature of TiO_2, it is considered safe for the environment. Additionally, when exposed to sunlight, TiO_2 is a powerful photocatalyst that produces the supra-band gap photon excitation, which improves the breakdown and

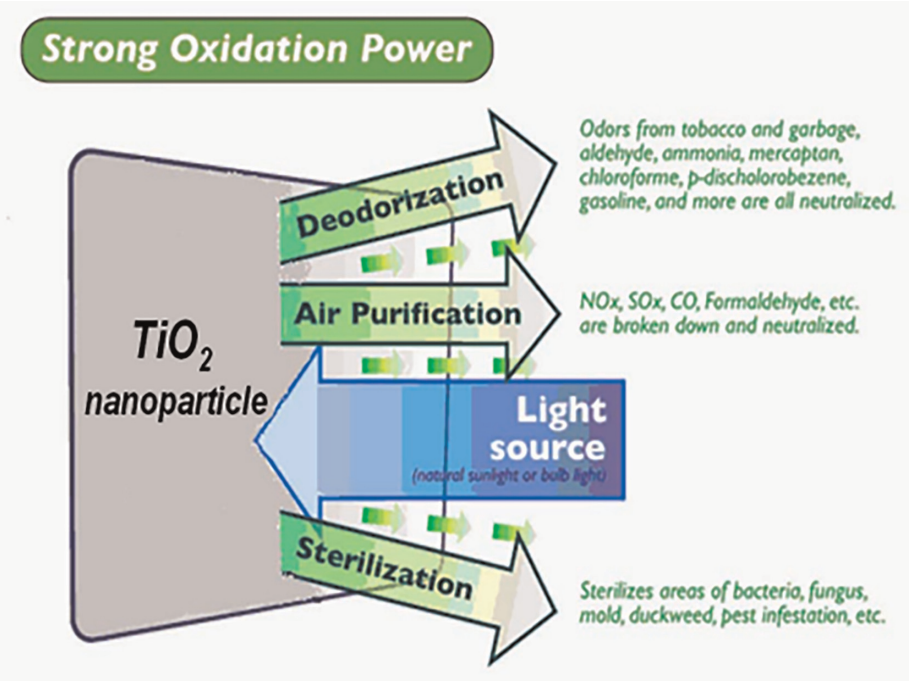

Figure 2.
Applications of titanium dioxide [9].

removal of inorganic matter that is hazardous like SO_2 in the atmosphere and environmental pollutants like NO_2 released into the air by exhaust gas [9].

2.2 Deodorization applications

TiO_2 excellent photocatalytic properties makes it suitable to be utilized in antibacterial and antiseptic compositions, where it breaks down organic pollutants and microorganisms. By breaking down the odor's source, which is ammonia and aldehyde gas (smoke), as shown in **Figure 3**, it essentially targets the source of the stench. When titanium dioxide is exposed to sunlight, it initiates a chemical reaction that breaks down organic poisons, smells, and other substances in the immediate vicinity [9].

2.3 Water purification applications

TiO_2 results in the breakdown of toxins produced by blue green algae and inhibition of other dangerous substances in water, leading to the elimination of organic matter from water, including organic chlorine compounds, trihalomethane, tetrachlorethylene, and methyl-tert-butyl ether trichloroethylene [10]. The following process illustrates how chloroform decomposes.

$$H_2O + CHCl_3 + (1/2)\, O_2 \rightarrow CO_2 + 3HCl \quad (1)$$

2.4 Pharmaceutical applications

TiO_2 photocatalyst can to break down cell membranes, harden virus proteins, and inhibit virus activation. In the pharmaceutical industry, it is frequently utilized to sanitize equipment that contains viruses. According to a study, TiO_2 can eradicate up to 99.97% of bacteria [11]. TiO_2 can eliminate mildew, suppuration fungus, green suppuration bacillus, and golden grape coccus. The golden grape coccus and coliform have been used to test the sterilizing process. At the start of the experiment, there were 3.2×10^5 golden grape coccus and 3.3×10^5 coliforms, but only 10 remained after the reaction with TiO_2 for 24 hours [11].

2.5 Photocatalytic application

Photons are emitted from the surface of a chemical compound that is light sensitive, when light strikes the compound, a chemical reaction known as photocatalysis

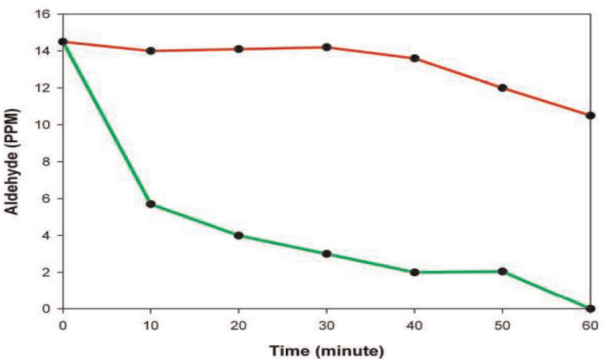

Figure 3.
Decomposition of aldehyde by titanium dioxide [9].

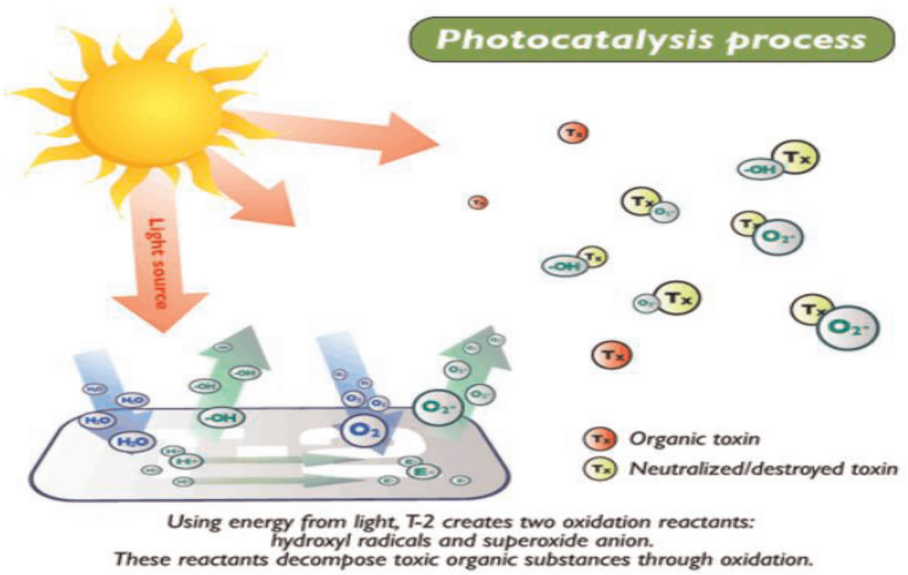

Figure 4.
Photocatalysis of titanium dioxide [9].

occurs. Photons with energy up to or greater than their band gap energy ($\lambda < 385$ nm) are absorbed by TiO_2 photocatalyst when exposed to light. A valence electron will be delocalized and excited to the semiconductor's conduction band as a result. Through one or more types of electron transfer processes, the photoexcited charge carriers can initiate the decomposition of the chemical species absorbed. They can, however, recombine radiatively or non-radiatively and release heat as a byproduct of the input energy, as shown in **Figure 4**. Additives can be added to TiO_2 to increase its efficiency by light illumination, thereby enabling it to become sensitive in the visible region with a decreasing band gap [9].

TiO_2 thin films have been the subject of much research because of their intriguing optical, electrical, and chemical features. TiO_2 nontoxicity and strong stability under light are properties that make it suitable as a dye-sensitized solar cell semiconductor [2, 3, 12, 13]. The most research material for DSSCs photoelectrode application is thin films of TiO_2 despite the existence of metal oxides such as SnO_2 and ZnO semiconductors with large band gaps. This is owing to its less susceptibility to photodegradation when exposed to sunlight. Moreover, the incident photon conversion efficiency (IPCE) and Isc, Voc, and η values are high in DSSCs fabricated using TiO_2 electrodes [14].

3. Properties of TiO_2

3.1 Physical properties of TiO_2

In nature, titanium oxide is found in abundance in mixture with other elements like iron. It can be found in trace levels in rocks that are sedimentary, igneous, and metamorphic. Black hexagonal crystals are the form that titanium dioxide nanoparticles exhibit. TiO_2 is the chemical formula for titanium dioxide, which has a composition of 40.55% oxygen and 59.55% titanium atoms [15]. The electronic configuration is displayed as follows:

Ti → [Ar] $3d^2 4s^2$.
O_2 → [He] $2s^2 2p^4$.

Having a density of 4.23 g/cm^3, a melting point of 1.843°C, and a boiling point of 2.972°C, it has a molar mass of 79.938 g/mol.

3.2 Crystal structural properties of TiO_2

Figure 1 depicted the three well-known titanium dioxides in crystalline phase: rutile, anatase, and brookite. Anatase and brookite are metastable, while rutile is very stable. **Table 1** shows the properties of these polymorphs and as a result of their varying properties, their photocatalytic activities also vary [1].

The space group Pbca describes the unit cell of brookite, which has eight formula units in the orthorhombic cell and an orthorhombic crystalline structure [8, 16, 17]. As seen in **Figure 5**, the formation of brookite can be seen as the connection of three distorted octahedral sharing edges of TiO_6, each with an oxygen atom at the corners and a titanium atom at the center. The crystal's proper chemical composition is provided by the octahedral's extensive sharing of edges and corners. The oxygen atoms are shown in two distinct places in the distorted octahedral [16]. Every titanium and oxygen atom has a distinct bond length [17]. The architecture of DSSCs has made extensive use of rutile and anatase polymorphs [13, 18], while brookite has received less attention and use due to its challenging synthetic process.

3.3 Semiconductor properties of TiO_2

When atoms of large groups come together to form a solid mass or molecules, atomic contact results in changing energy levels because of the mass quantities of

	Lattice parameter (Å)	Space group	System type	Energy band gap (eV)
Rutile	a = 4.594 c = 2.958	$P4_2/mnm–D_{4h}^{14}$	Tetragonal	3.0
Anatase	a = 3.784 c = 9:515	$I4_1amd–D_{4h}^{19}$	Tetragonal	3.4
Brookite	a = 9.166 b = 5.436 c = 5.135	$Pbca – D_{2h}^{15}$	Orthorhombic	3.3

Table 1.
Properties of rutile, brookite, and anatase polymorphs of TiO_2.

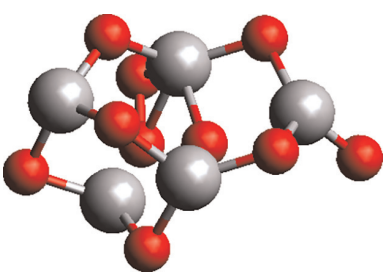

Figure 5.
$(TiO_2)_5$ brookite nanocluster.

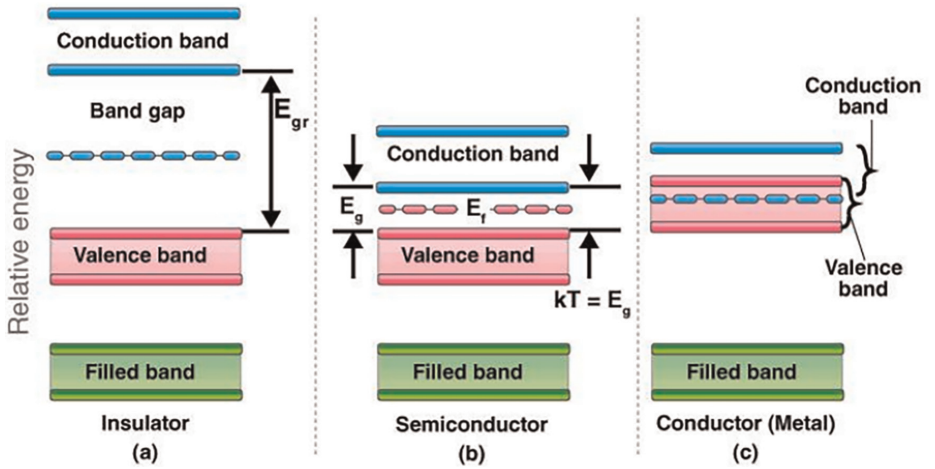

Figure 6.
Valence bands (pink), conduction bands (blue), band gaps, Fermi energy levels for insulators, semiconductors, and conductors Eq. (1).

distinct molecular orbitals, which may be near or even entirely degenerate. Electrons in an isolated atom have definite, defined energy levels. It is claimed that these energy levels form continuous energy bands. The valence band (VB) is the energy band in the highest energy molecular orbital (HOMO) that contains all of the valence electrons. It can be filled entirely or partially. The energy band where mobile charge carriers, either positive or negative, are present is the conduction band (CB). EV stands for the greatest attainable valence-band energy, and EC stands for the lowest attainable conduction-band energy. **Figure 6** shows an illustration of the energy of the band gap, also known as the band gap (EG), which is the difference in energy between the margins of these two bands.

$$E_G = E_C - E_V \tag{2}$$

The conduction band is empty, and the valance band is full at low temperatures. Whereas mobile charge carriers that are negative are electrons, positive mobile charge carriers are holes. The process of conduction in semiconductor materials begins when electrons get sufficient energy to leave a hole in the valence band and jump into the conduction band, where they can flow freely within the crystal lattice [19].

The highest occupied energy level is located at the border between the conduction and the valence in metals, as depicted in **Figure 6**. Very little energy is required by electrons at the top of the valence band to escape into the conduction band [19]. There is a wide energy gap between the conduction bands and valence bands in insulators. It is typically impractical to gain enough energy to excite electrons from the valence band to the conduction band due to the forbidden gap, which is on the order of a few electron volts. Atomically tiny energies are produced in a material via thermal excitations and typical electric circuit voltages. In insulators, the energy difference between the valence and conduction bands cannot be filled with this amount of energy. Semiconductors can be made more conductive by adding tiny amounts of doping material. As a result, the band gap between the valence and conduction bands narrows, leading to a noticeable increase in conductivity. Charge carriers, namely electrons and holes, define semiconductors. The charge carriers show conductivity that is halfway

between that of insulators and conductors. They have resistivity in the range of 10^9–10^{-2} Ωcm [20]. As temperature rises, there is an increase in concentration of free electrons and holes. Intrinsic semiconductors, such as silicon and germanium, conduct in chemically pure states.

3.3.1 Direct and indirect band gaps

Phonons and photons interactions (holes and electrons) and energy-momentum (E-k) relationship for carriers in a lattice where momentum and energy must be conserved lead to the concepts of band gaps. Schrödinger equation of an approximate one-electron problem shown in Eq. (4) is solved in order to estimate the energy-momentum (E-k) relationship, or the band structure of a crystalline solid [21].

$$\left(\frac{-h^2}{2m}\nabla^2 + V(R)\right)\varphi(r,k) = E(k)\varphi(r,k) \tag{3}$$

For semiconductor material to be applied in solar cells, lasers, thermoelectric devices, and electronic devices, its band gap is essential. Direct and indirect band gaps are the two types of band gaps seen in semiconductors. In direct-band gap semiconductors, the valance band maximum and conduction band minimum are situated at the same momentum (k) values, as shown in **Figure 7**. There would not be change in momentum values when a hole at the top of the VB recombines with an electron at the bottom of the CB. Radiative transitions are those in which energy is conserved by means of photon emission. As seen in **Figure 3**, the CB minimum and VB maximum in indirect band gap material are located at distinct k-values. Phonons are required for conservation of momentum during the recombination of an electron and a hole in an indirect-band gap semiconductor material [22, 23].

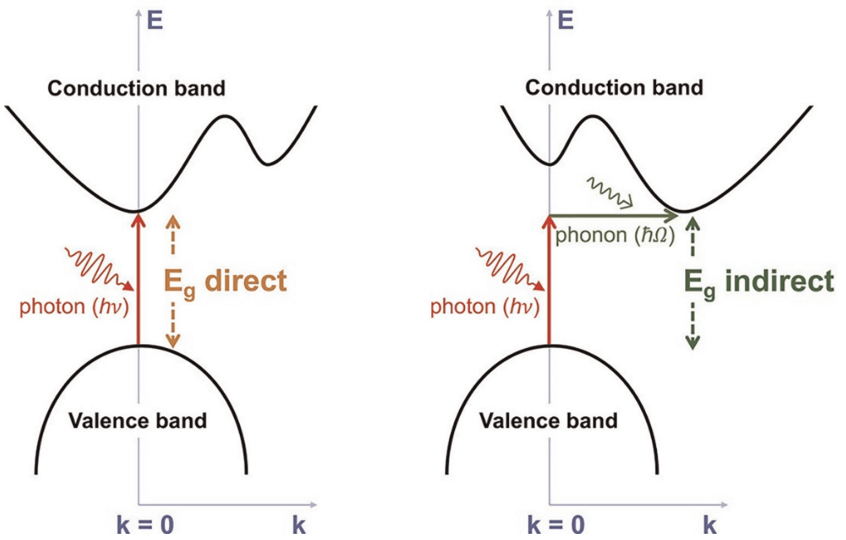

Figure 7.
Photon emission in direct and indirect band gap semiconductors [22].

3.3.2 Fermi levels in semiconductors

A semiconductor material's conduction band is made up of numerous permitted empty energy levels. The likelihood that an electron will fill a level with energy E at thermal equilibrium is represented by the Fermi-Dirac distribution function, or f (E). The Fermi-Dirac distribution function f (E) can be expressed using this (Eq. (4)):

$$f(E) = \frac{1}{1 + exp\left(\frac{E-E_F}{k_B T}\right)} \tag{4}$$

where T is the temperature in Kelvin, E_F is the Fermi energy or Fermi level, and k_B is Boltzmann's constant. Fermi energy is the electrochemical potential of the electrons in a semiconductor material. It stands for the material's average electron energy. The chance that an electron will occupy an energy level E is represented by f(E), but the probability that it will remain empty or that it will have an equivalent hole in the valence band is represented by (1-f(E)) [24].

3.3.3 Density of states and carrier concentration

An energy band is a collection of discrete energy states. Every state in quantum physics corresponds to a unique spin (up and down) and unique solution to the Schrödinger's wave equation for the periodic electric potential function of the semiconductor [22]. The number of electrons (occupied conduction-band levels) for an intrinsic semiconductor is given by Eq. (6), which is the total number of states N(E) multiplied by the occupancy F (E), integrated over the conduction band as presented in (Eq. (5)).

$$n = \int_{E_c}^{\infty} N(E)F(E)dE \tag{5}$$

None or one electron can be present in each state. The density of states, as provided by (Eq. (6)), is the number of states in a narrow range of energy ΔE in the energy bands.

$$D(E) = \frac{numberofstates \in \Delta E}{\Delta E \times Volume} \tag{6}$$

The valence-band VB and conduction-band CB's density of states, denoted by Dc and Dv, respectively, are functions of E, the location of ΔE, according to (Eqs. (7) and (8)).

$$D_c(E) = \frac{8\pi m_n \sqrt{2m_n(E - E_c)}}{h^3} E \geq E_C \tag{7}$$

$$D_v(E) = \frac{8\pi m_p \sqrt{2m_p(E_v - E)}}{h^3} E \leq E_v \tag{8}$$

where mn and mp are electrons and holes effective masses, respectively, averaging over a number of orientations to account for anisotropy. Dc(E) and Dv(E) have

dimensions of one number per cubic centimeter per electron Volt. The products Dc (E) dE and Dv(E) dE represent the number of energy levels in the energy range between E and E + dE per cubic centimeter of the semiconductor volume. The separation of charge carriers in semiconductors and the photovoltaic effect are the principles that govern the production of electricity by photovoltaic technology.

TiO_2 performs better as a photocatalyst in nanoparticle form than in bulk structure; extensive research indicates that the charge carrier of a crystalline semiconductor particle behaves quantum mechanically like a simple particle in a box when its diameter is lowered to a threshold radius of 10 nm [25]. Quantized semiconductor particles are more photoactive than microcrystalline semiconductor particles, according to Mill and Le Hunte [26]. This is because the absorption edge blue shifts as particle size decreases, raising the redox potential of the particle's photogenerated holes and electrons.

4. Adsorption of dyes to TiO_2 surfaces and anchor group

One or more anchoring groups anchor dyes to the surface of nanocrystalline semiconductors. The adsorption modes that dyes append to the TiO_2 surface and the electronic coupling that takes place between the dye-excited states and the unoccupied states of the semiconductor are factors that determine the efficiency of DSSCs. There are several methods in which adsorbate oxygen atoms and surface metal atoms can bond an adsorbate to a metal oxide surface. The molecule can bind itself to the surface metal atom via mono (1 M), bi (2 M), or tridentate (3 M) coordination. When there are several metal-oxygen linkages, the number of metal atoms (1 M, 2 M) involved in the adsorption process can also be utilized to differentiate between the adsorption modes.

The most employed anchor groups for attaching sensitizers to semiconductor surfaces are phosphonic acid and carboxylic acid [27, 28]. Some of the potential configurations for the different carboxylic acid adsorption modes are depicted in **Figure 8**.

Recent research on the adsorption of dyes comprising of carboxylic on TiO_2 surfaces indicates that bidentate bridging (BB), shown in **Figure 8c**, is the most favorable adsorption mechanism. In this adsorption mode, one proton is transferred to a neighboring surface oxygen [27, 30–32].

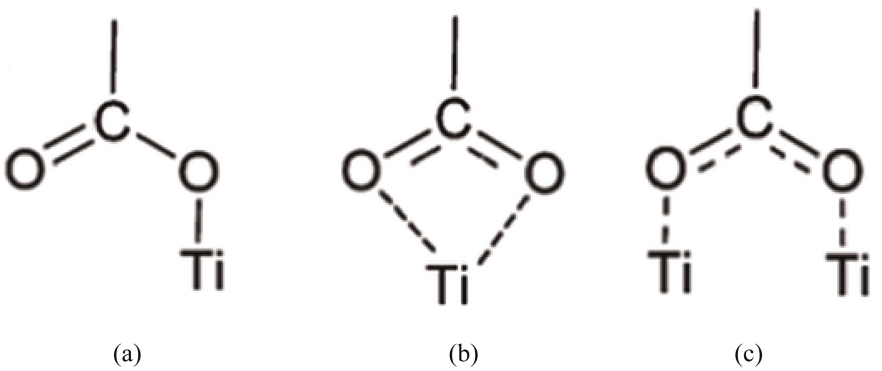

Figure 8.
(a) Monodentate, (b) bidentate chelating, and (c) bidentate bridging [29].

5. Review of related works

Studies using density functional theory on the surfaces of brookite (210) and anatase (101) showed that the building blocks of the two surfaces are comparable. One of the most relaxed and stable surfaces of brookite polymorphs is the brookite (210) surface [33].

A comprehensive density functional theory study on the adsorption geometry of Ru and YE05 sensitizer on TiO_2 substrate for DSSC application was published by Fillipo et al. [30]. The results showed that the dyes functionalized with four carboxylic groups and contained two bipyridine ligands absorbed onto the TiO_2 surface through these carboxylic groups [30].

Density functional theory was used by Prajongtat et al. [34] to examine the electronic and structural characteristics of eight distinct azo dyes (Ar-N=N-Ar, where Ar and Ar′ indicate the aryl group, including benzene and naphthalene skeletons) as well as their absorption into anatase TiO_2. The adsorption energies obtained show that the adsorbed dyes preferentially adopt chelating or monodentate geometries over bidentate bridging configurations. Additionally, the azo compounds containing two carboxyl groups are more selectively coupled to the TiO_2 surface, with the carboxyl group connecting to the benzene moiety rather than the naphthalene moiety [34].

Babara et al. used a vacuum spectrometer and vacuum-tight attenuated total reflection infrared (ATIR-IR) to measure the impact of the anchor and backbone of perylene dye molecules as well as the infiltration of dye molecules unto porous TiO_2 film at a high degree of sensitivity. Their findings showed that dyes with anhydride groups absorb less readily to thin films than dyes with acidic anchor groups. Overall, the simulation findings indicate that the anchoring group has a major effect on the rate of adsorption [35].

With the aid of computer simulations and FT-IR measurements, Chiara et al. examined the energetically favorable TiO_2-adsorption mode of acetic acid as a helpful model for real-world organic dyes. The findings showed that a bridging bidentate adsorption mode was the most durable binding, closely matching the Fourier Transform Infrared Spectroscopy (FT-IR) frequency pattern, for real organic dyes with cyanoacrylic anchoring groups. While the bridging bidentate mode produced a stronger coupling and faster electron injection, the undissociated monodentate adsorption mode for the rhodamine-3-acetic acid anchoring group was shown to be comparably stable. The investigation revealed a relationship between the different electron injection/recombination properties of the oxidized dye and the structural changes caused by the different anchoring groups [36].

Jun et al. [37] investigated alkaline earth metal Ca and N co-doped anatase TiO_2 sheets with exposed (001) facets made using hydrothermal methods. It was confirmed by the X-ray diffractometer and X-ray photoelectron spectroscopy results that the N monodoped TiO_2 is less crystallin than the Ca and N co-doped TiO_2. The study confirms that co-doping Ca and N can successfully lower the generation of recombination centers, increase the efficiency of separating photo-induced electrons and holes, and improve TiO_2's photocatalytic activity based on the hydroxyl radicals (OH) produced during the photocatalytic experiment [37].

In order to alter the photoelectrochemical characteristics of anatase TiO_2, Xu et al. investigated co-doped anatase TiO_2 with transition metals (V or C) and non-metals (N or C). First principles plane wave ultrasoft pseudopotential calculations were used to evaluate the stability and visible light photoactivity, formation energies of the

dopant and electronic structures. The results of the investigation demonstrated that co-doping with transition metals makes it easier to increase the p-type dopant concentration. In addition to maintaining the edge of the conduction band oxidation–reduction potential, compensated co-doping lowers the energy gap, increases optical absorbance, improves carrier mobility, and increases conversion efficiency [38].

Puyad et al. studied two model croconate dyes, designated CR1 and CR2, one with an electron-donating substituent (CR1) and the other with an electron-withdrawing group (CR2). They used the periodic density functional theory to study the adsorption of the diketo (-COCO-) groups on the surface of stoichiometric TiO_2 anatase (101). Their findings showed how strongly the acidic group (-COOH) could adhere to the surface of TiO_2. Further theoretical studies also anticipated that the binding strength of the diketone group would be substantial and comparable to that of the -COOH group. This causes a competitive binding of the acid groups on the TiO_2 surface and the diketone groups of croconate dyes [39].

Reports on two croconate dyes, CR1 and CR2, were provided by Chitumalla et al. The researchers used periodic density-functional theory (DFT) simulations and density functional theory to calculate the electrical and optical properties of these dyes. They also examined the adsorption behavior of the two dyes on the TiO_2 (101) anatase surface. Periodic and electronic-structure calculations show that the diketone group of CR1 bonds to the TiO_2 surface more strongly than that of CR2, with a binding strength comparable to that of a typical organic dye. The substituent has a major effect on the croconate dyes' adsorption, optical, and electrical properties [40].

Leonardo et al. [41] reported a periodic density study of a tertiary trimethylamine adsorption on the three most exposed surfaces of stoichiometric anatase TiO_2 nanorods. Following an investigation and characterization of the energetic, structural, and electrical properties, it was found that trimethylamine introduced unique molecular states close to the edge of the TiO_2 valence band [41].

Density functional theory was used by Hao Yang et al. [12] to examine the ruthenium (N3) sensitizer's adsorption behavior on the anatase TiO_2 (001) surface. According to the study's findings, N3 interacts with the (001) surface more strongly than the (101) surface, which causes the (001) surface to have a higher dye coverage. When the N3 sensitizer was adsorbed, its energy gap was reduced, indicating a wider absorption spectra range than when the N3 sensitizer was separated. Furthermore, it was discovered that the TiO_2 (001) surface had a greater conduction band minimum than the TiO_2 (101) surface, indicating a higher open circuit voltage. The findings provided helpful hints and insight into the excellent solar to power DSSCs conversion efficiency including exposed surface TiO_2 (101) nanocrystals [12].

Monique et al. investigated the CO_2 interactions with the (210) surface of brookite TiO_2 by means of first principle simulations on cluster and periodic slab systems. Charge spin density tests were performed to determine the charge transfer to the CO_2 molecule, and the results were compared with the charge transfer to the anatase TiO_2 (101) surface. The study found that the anatase (101) surface and the brookite (210) surface provide CO_2 interactions that are equal in terms of energy. The findings suggested that increasing the amount of oxygen vacancies on the brookite surface might enhance CO_2 absorption. Large levels of CO_2 are verified to be present in the oxygen-deficient brookite based on diffuse reflectance-generated laboratory data and Fourier transform infra-red spectroscopy [33].

Elegbeleye et al. investigated the electronic state energy, optical properties, and energy level alignment of the ruthenium (N3) sensitizer adsorbed on brookite TiO_2 cluster in order to comprehend the electron injection efficiency and kinetics of the

dye/TiO_2 complex. The light absorption maximum red shifting to higher wavelength was attributed to the ruthenium N3 dye's absorption on a brookite cluster, which resulted in the distribution and shifting of the lowest unoccupied molecular orbital (LUMO) from the dye to the TiO_2 cluster. The results indicated that the dye-stimulated state of TiO_2 semiconductors can benefit from favorable electron injection. Based on their findings, TiO_2 brookite has the potential to become a new candidate in the DSSC semiconductor market [42].

Many investigations on surface modification of TiO_2 crystals employing atoms or sensitizing dye molecules have been carried out in order to lower the band gap and boost the activity of TiO_2 crystals in the visible and near-infrared parts of the solar spectrum. Anatase and rutile polymorphs of TiO_2 have been used as models in these kinds of studies to improve photocurrent yield and light harvesting in DSSC [12, 24]. The results showed enhanced spectrum responsiveness and increased TiO_2 photocatalytic capabilities. TiO_2 oxide basic research has made substantial use of the surfaces of anatase and rutile polymorphs, which have been employed as a paradigm. The rutile and anatase polymorphs of TiO_2, which are widely used, have been investigated extensively, while the brookite form has gained little or no attention [13].

An investigation on TiO_2 brookite recently suggests that TiO_2 brookite might have higher photocatalytic activity [13]. According to a previous study, brookite's absorption edge is wide and reaches the visible region of the solar spectrum, in contrast to the sharp edges in the visible displayed by the TiO_2 rutile and anatase polymorphs. Considering the dearth of studies on brookite surfaces and their alleged enhanced photocatalytic properties, optimizing photon current density in dye-sensitized solar cells via investigation of dye-brookite TiO_2 interactions is highly desirable.

6. Optical and electronic properties of TiO_2 brookite clusters

6.1 Computational procedures

Using Materials Studio BIOVIA, the bulk structure of the brookite TiO_2 exported from the CASTEP module was optimized to obtain the ground-state structure of the TiO_2 brookite semiconductor [43]. 4x7x7 and 650 eV, respectively, were the convergence energy cut-off and k-points employed for this study. An optimal ground state bulk structure was cleaved to obtain three brookite clusters. The modeled clusters that were cleaved are (i) a brookite nanocluster of size 5 Å in x, y, and z directions; (ii) a cluster with a stoichiometry of $(TiO_2)_n$, where n = 8; and (iii) a cluster with a stoichiometry of (TiO_2) n, where n = 68. Repeating the unit cell supercell by 2 x 2 x 2 Å in the x, y, and z directions led to the formation of $(TiO_2)_{n=68}$ cluster. All the structures were viewed using Avogadro software and exported to GPAW software via the crystallographic information format (cif), for further calculations and analysis.

All DFT calculations were executed within an atomic simulation environment (ASE) using GPAW software [44]. Avogadro was used to display the formations. GPAW is a computer package written in Python that combines the grid space projector-augmented wave (GPAW) with density-functional theory (DFT). **Figures 5–10** show the three TiO_2 brookite clusters that were considered for this study. As mentioned in the preceding section, **Figure 5** shows a $(TiO_2)_5$ brookite nanocluster made up of ten oxygen atoms and five titanium atoms that have been cleaved from the bulk structure of brookite. The structure of brookite $(TiO_2)_8$, which

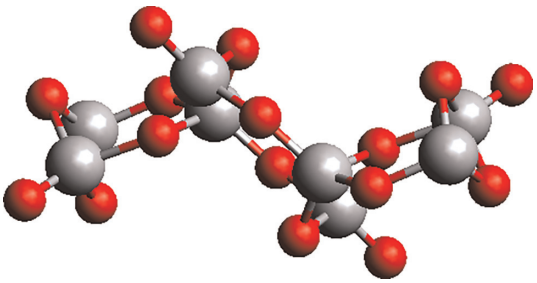

Figure 9.
$(TiO_2)_8$ brookite cluster.

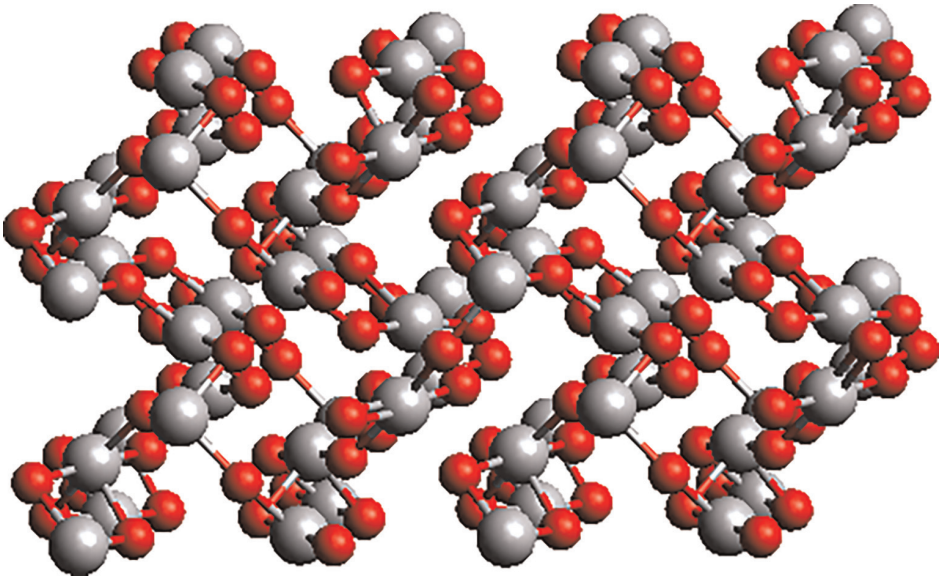

Figure 10.
$(TiO_2)_{68}$ brookite supercell.

is composed of eight titanium and sixteen oxygen atoms, is shown in **Figure 9**. The structure was imported into the Avogadro visualizing interface using the crystallographic mode (cif) without periodicity. A periodic brookite $(TiO_2)_{68}$ supercell measuring 2 x 2 x 2 Å is shown in **Figure 10**. It is made of 136 oxygen atoms and 68 titanium atoms. A cluster or supercell of any size can be formed by repeating unit cells in the x, y, and z directions, which together make up the bulk structure known as the periodic structure.

With the PBE exchange correlation functional, GPAW was used to relax each structure in vacuum. The structures were taken to have converged when all of the atoms were exposed to maximal stresses of roughly 0.05 eV for the non-periodic brookite $(TiO_2)_5$ and $(TiO_2)_8$ cluster models. In the relaxation process, the periodic boundary conditions were applied to the supercell. The atoms in the cluster were rearranged during the relaxing process until the ground state configuration was reached, where the forces converged to a maximum of 0.05 N and the cluster was stable. The nanocluster structures' UV/Vis, total density of states, and partial density of states were computed using the trajectory data obtained from the relaxed

structures. The Total Density of States (TDOS) and Partial Density of States (PDOS) from the GPW files were computed using the Perdew–Burke–Ernzerhof (PBE) functional, and the UV/Vis was calculated in vacuum.

6.2 Optical properties of $(TiO_2)_5$ and $(TiO_2)_8$ brookite clusters

The absorption spectra of the $(TiO_2)_5$ and $(TiO_2)_8$ brookite clusters were simulated in vacuum using the TD-DFT method. The TD-DFT calculations were performed while using the PBE exchange correlation functional. The absorption spectra of $(TiO_2)_{68}$ was not computed due to its periodicity. The UV/Vis absorption spectra of $(TiO_2)_5$ brookite nanoclusters and $(TiO_2)_8$ brookite clusters are displayed in **Figures 11** and **12**, respectively. The absorption spectra of $(TiO_2)_5$ seen in **Figure 11** were computed using the hybrid density functional theory B3LYP approximation, and the GPAW was employed to construct the absorption spectra of the complex depicted in **Figure 11** using the PBE exchange correlation functional. The results indicate that both $(TiO_2)_5$ and $(TiO_2)_8$ brookite clusters display absorption in the UV region.

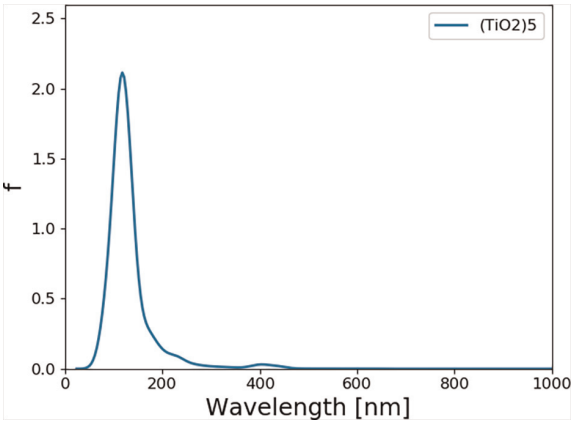

Figure 11.
UV/Vis absorption spectrum for $(TiO_2)_5$ brookite cluster.

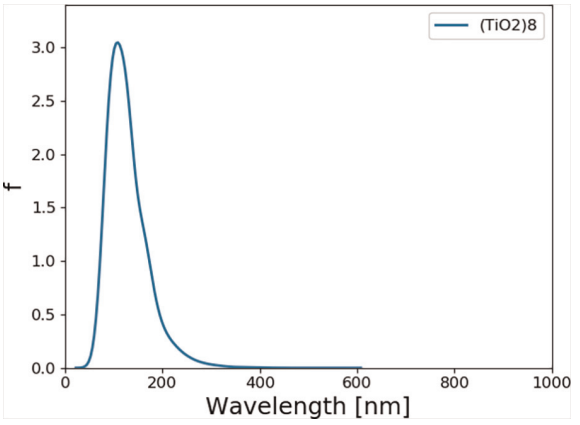

Figure 12.
UV/Vis absorption spectrum for $(TiO_2)_8$ brookite cluster.

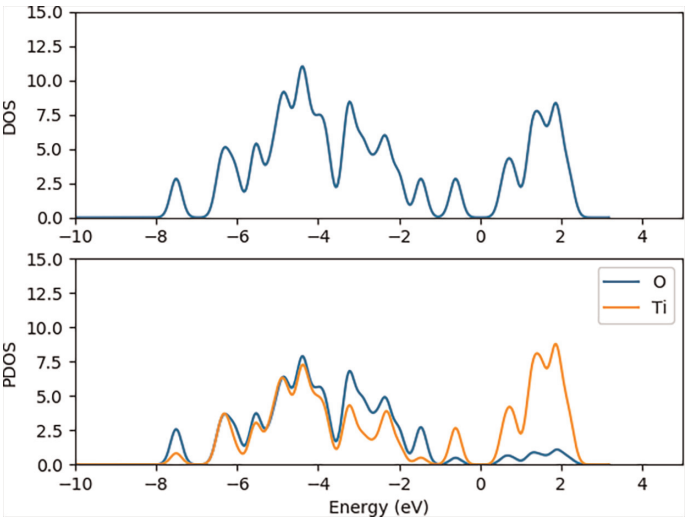

Figure 13.
TDOS (upper) and the estimated DOS (lower) for the $(TiO_2)_5$ nanocluster, where the blue line represents the oxygen contributions to PDOS and the red line represents the titanium atom contributions.

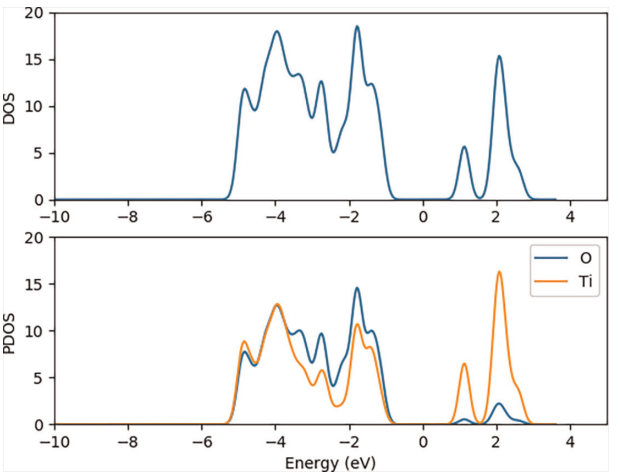

Figure 14.
TDOS (upper) and the estimated DOS (lower) for the $(TiO_2)_8$ nanocluster, where the blue line represents the oxygen contributions to PDOS and the red line represents the titanium atom contributions.

Figure 11 shows more prominent peaks, although this might be because a different functional was used to compute the absorption spectra. $(TiO_2)_5$ and $(TiO_2)_8$ brookite clusters, both show absorption in the UV region of the solar spectrum as shown in **Figures 11** and **12**. Although $(TiO_2)_5$ displays a small absorption peak at 400 nm, notable absorption peaks were mostly situated at 200 nm. An increased peak height observed for $(TiO_2)_8$ brookite absorption spectra relative to the $(TiO_2)_5$ absorption spectra indicates higher absorbance. Due to the wide band gap (3.0–3.2 eV), the absorption spectra of $(TiO_2)_5$ and $(TiO_2)_8$ demonstrate that TiO_2 is primarily sensitive in the UV region of the solar spectrum, which is generally consistent with findings from literature [16].

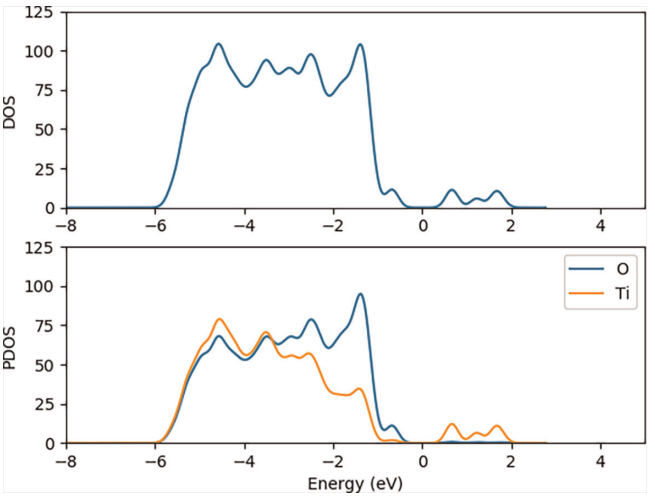

Figure 15.
TDOS (upper) and the estimated DOS (lower) for the $(TiO_2)_{68}$ nanocluster, where the blue line represents the oxygen contributions to PDOS and the red line represents the titanium atom contributions.

6.3 Electronic properties of (TiO_2) n n = 5, 8, 68 brookite clusters

The density of states and projected density of states were computed using GPAW and PBE exchange correction functional in order to better understand the electronic structure of the $(TiO_2)_5$, $(TiO_2)_8$, and $(TiO_2)_{68}$ nanoclusters. The TDOS and PDOS shown in **Figures 13–15** denote the total and partial density of states for $(TiO_2)_5$, $(TiO_2)_8$, and $(TiO_2)_{68}$, respectively. The DOS illustrates the wide band gap that separates the surface valence and conduction bands.

The PDOS signatures for the clusters show that the valence state contributions emanate from the oxygen and titanium atomic orbitals. **Figures 10–12** illustrates that the oxygen 2p atomic orbitals contribute mostly to the highest occupied valence band (VB) state, while the titanium 3d atomic orbitals predominantly contribute to the lowest unoccupied state of the conduction band. With the exception of a tiny amount from the titanium p atomic orbitals, the oxygen p atomic orbitals predominate the valence band. The bulk of the titanium orbitals, especially the d and p ones, contribute to the conduction band; the contributions of the oxygen atoms are minimal.

7. Conclusion

TiO_2 is suited for industrial, environmental, medicinal, deodorization, photovoltaic, and water purification applications due to its intriguing physical, chemical, optical, electronic, and spectrum properties. Rutile and anatase polymorphs of TiO_2 have been thoroughly investigated and used in a variety of applications, particularly for the fabrication of photoanodes for dye-sensitized solar and hybrid organic and inorganic solar cells. As far as we are aware, not much research has been conducted on brookite TiO_2, which has limited its potential for broad use as a semiconductor in solution-processed-based metal organic and hybrid organic–inorganic solar cell device

architecture, as well as DSSC photoanodes. Extensive research is required to completely comprehend TiO_2 brookite polymorphs' UV–Vis absorption, electronic excitation energies, and light harvesting efficiency, as well as the related adsorption on dye molecules. Enhancing their optoelectrical and industrial applications will require more knowledge about the optical and electronic properties of the dye/brookite TiO_2 complex. These properties include their formation energies, UV–Vis absorption, HOMO-LUMO energy levels and energy gap, energy level alignment and free energy of electron injection, density of states and projected density of states, photon current densities, and I-V characteristics. Optimizing the optical characteristics of the dye/brookite TiO_2 interface will help to increase the photon to current conversion efficiencies and gain a better knowledge of the absorption mechanisms. This can be accomplished by the thorough study of the TiO_2 brookite polymorph.

Acknowledgements

We express our gratitude to the BwForCluster for Neuroscience, Elementary Particle Physics, and Microsystems Engineering (NEMO), Freiburg, Germany, as well as the Center for High Performance Computing in Cape Town, South Africa, for providing the computational resources needed to implement this study. This chapter was adapted from my dissertation titled "Studies of Interaction of Dye Molecules with TiO_2 Brookite Clusters for Dye-Sensitized Solar Cells Application".

Author details

Ife Elegbeleye[1*], Edwin Mapasha[1], Eric Maluta[2] and Regina Maphanga[3]

1 Department of Physics, University of Pretoria, South Africa

2 Department of Physics, University of Venda, Thohoyandou, South Africa

3 Council for Science and Industrial Research, Pretoria, South Africa

*Address all correspondence to: ifelove778@gmail.com

IntechOpen

© 2025 The Author(s). Licensee IntechOpen. This chapter is distributed under the terms of the Creative Commons Attribution License (http://creativecommons.org/licenses/by/4.0), which permits unrestricted use, distribution, and reproduction in any medium, provided the original work is properly cited. CC BY

References

[1] Sungur Ş. Titanium Dioxide Nanoparticles. In: Kharissova OV, Torres-Martínez LM, Kharisov BI, editors. Handbook of Nanomaterials and Nanocomposites for Energy and Environmental Applications. Cham: Springer;; 2021. pp. 3-9. DOI: 10.1007/978-3-030-36268

[2] Nyiko MC, Mpfunzeni R. A review: Simultaneous "one-pot" pollution mitigation and hydrogen production from industrial wastewater using photoelectrocatalysis process. Materials Today Catalysis. 2024;**5**:10052. DOI: 10.1016/j.mtcata.2024.100052

[3] Hayat K, Mansoor UHS. Modification strategies of TiO_2 based photocatalysts for enhanced visible light activity and energy storage ability: A review. Journal of Environmental Chemical Engineering. 2023;**11**:111532. DOI: 10.1016/j.jece.2023.111532

[4] Armakovi'c SJ, Savanovi'c MM, Armakovi'c S. Titanium dioxide as the Most used Photocatalyst for water purification: An overview. Catalysts. 2023;**13**:1-29. DOI: 10.3390/catal13010026

[5] Chauke NM, Mohlala RL, Ngqoloda S, Raphulu MC. Harnessing visible light: Enhancing TiO_2 photocatalysis with photosensitizers for sustainable and efficient environmental solutions. Frontiers in Chemical Engineering. 2024;**6**:1-25. DOI: 10.3389/fceng.2024.1356021

[6] Jafari S, Mahyad B, Hashemzadeh H, Janfaza S, Gholikhani T, Tayebi L. Biomedical applications of TiO_2 nanostructures, recent advances. International Journal of Nanomedicine. 2020;**15**:3447-3470. DOI: 10.2147/IJN.S249441

[7] Material Studio Accerlrys. Dassault Systèmes. BIOVIA. 2016

[8] Diebold U. Structure and properties of TiO_2 surfaces: A brief review. Application Physics. 2003;**76**:681-687. DOI: 10.1007/s00339-002-2004-5

[9] Behzad R, Hamid M. Applications of titanium Dioxdie Nanocoating. Nano-Technology in Environments Conference. 2006:1-3

[10] Ollis DF, Al-Ekabi H. Photocatalytic Purification and Treatment of Water and Air. Elsevier. 1993:511-532

[11] John CI, Petra K, Eugene WR, Robert MC. Inactivation of Escheria coli by titanium dioxide photocatalytic oxidation. Applied and Environmental Microbiology. 1993;**59**:1668-1670

[12] Hao Y, Jia L, Gang Z, Sum WC, Hongda D, Lin G, et al. First principles study of ruthenium (II) sensitizer adsorption on anatase TiO_2 (001) surface. Royal Society of Chemistry Advances. 2015;**5**:60230-60236

[13] Raghvendra SD, Sandesh RJ, Ajinkya BB. Synthesis and characterization of various doped TiO_2 nanocrystals for dye-sensitized solar cells. ACS Omega. 2021;**6**:3470-3482. DOI: 10.1021/acsomega.0c01614

[14] Bandaranayake KMP, Senevirathna MKI, Weligamuwa PMGMP, Tennakone K. Dye sensitized solar cells made from nanocrystalline TiO_2 films coated with outer layers of different oxide materials. Coordination Chemistry Reviews. 2004;**248**:1277-1281. DOI: 10.1016/j.ccr.2004.03.024

[15] DuPont. Titanium Oxide (Titania, TiO_2) Nanoparticles Properties, Applications. AZoNano. 2013. 1-3

[16] Sumaiya IS, Shanawaz A, Allah RA, Sharif Md A. Crystallographic biography on nanocrystalline phase of polymorphs titanium dioxide (TiO_2): A perspective static review. South African Journal of Chemical Engineering. 2024;**50**:51-64. DOI: 10.1016/j.sajce.2024.07.005

[17] Elegbeleye IF, Maluta NE, Maphanga RR. Density functional theory study of optical and electronic properties of $(TiO_2)_{n=5,8,68}$ clusters for application in solar cells. Molecules. 2021;**26**:1-19. DOI: 10.3390/molecules26040955

[18] Di Paola A, Bellardita M, Palmisano L. Brookite, the least known TiO_2 Photocatalyst. Catalysts. 2013;**3**: 36-73

[19] Md AA, Md AS. Semiconductors. International Journal of Advance Multidisciplinary Research. 2020;**7**:1-8. DOI: 10.22192/ijamr.2020.07.04.001

[20] Kashy ER, Frank NH, Suckling EE, McGrayne SB, Electricity. Encyclopedia Britannica. 2024. Available from: https://www.britannica.com/science/electricity

[21] Sze S, Ng KK. Physics of Semiconductor Devices. Third ed. John Wiley & Sons, Inc; 2007. pp. 1-815. DOI: 10.1002/0470068329

[22] Pedro HMA, Volkringer C, Loiseau T, Tejeda A, Hureau M, Moissette A. Band gap analysis in MOF materials: Distinguishing direct and indirect transitions using UV–vis spectroscopy. Applied Materials Today. 2024;**37**:1-15. DOI: 10.1016/j.apmt.2024.102094

[23] Kelechi I, Chinenye U, Onwumelu AI. The Use of Wide Band Gap Semiconductors in the Production of Electronic Devices and its Feasibility Study in Nigeria – Review. International Journal of Advanced Science and Engineering . 2023;**10**:3410-3421. DOI: 10.29294/IJASE.10.2.2023.3410-3421

[24] Chenming H. Electrons and Holes in Semiconductors. 2009. 1-34

[25] Shikha V. A review on different method of preparation of TiO2 nanoparticles. International Journal of Scientific Research and Review. 2019;**8**: 518-535

[26] Mills A, Hunte SL. An overview of semiconductor photocatalysis. Journal of Photochemistry and Photobiology. 1997; **108**:1-35. DOI: 10.1016/S1010-6030(97)00118-4

[27] Du K, Wang A, Li Y, Xu Y, Li L, Yuan N, et al. The synergistic effect of Phosphonic and carboxyl acid groups for efficient and stable perovskite solar cells. Materials. 2023;**16**:1-11. DOI: 10.3390/ma16237306

[28] Lunlun G, Heng Y, Chengming N, Xuran S, Xiuli W, Mei W. Influence of anchoring groups on the charge transfer and performance of p-Si/TiO_2/Cobaloxime hybrid photocathodes for Photoelectrochemical H_2 production. ACS Applied Material and Interfaces. 2019;**11**:34010-34019. DOI: 10.1021/acsami.9b12182

[29] Adineh M, Pooya T, Mohsen A, Nasser S, Ezeddin M. Fabrication and analysis of dye-sensitized solar cells (DSSCs) using porphyrin dyes with catechol anchoring groups. RSC Advances. 2016;**6**:14512-14521. DOI: 10.1039/c5ra23584g

[30] Fillippo DA, Simona F, Annabella S, Mohammad KN, Michael G. First-principles modelling of the adsorption geometry and electronic structure of Ru

(II) dyes on extended TiO_2 substrates for dye-sensitized solar cell application. Journal of Physical Chemistry. 2010;**114**: 6054-6061. DOI: 10.1021/jp911663k

[31] Nadeem IM, Hargreaves L, Harrison GT, Idriss H, Shluger AL, Thornton G. Carboxylate adsorption on rutile TiO_2(100): Role of coulomb repulsion, relaxation, and steric hindrance. Journal of Physical Chemistry C Nanomaterial Interfaces. 2021;**125**: 13770-13779. DOI: 10.1021/acs.jpcc.1c00892

[32] El-Zohry AM, Agrawal S, De Angelis F, Pastore M, Zietz B. Critical role of protons for emission quenching of Indoline dyes in solution and on semiconductor surfaces. Journal of Physical Chemistry C Nanomaterial Interfaces. 2020;**124**:21346-21356. DOI: 10.1021/acs.jpcc.0c07099

[33] Mengmei P, Niu H, Xingzhang ZJ, Xiaoli Z. Enhanced efficiency of dye sensitized solar cell by high surface area anatase TiO_2 modified P25 paste. Journal of Nanometals. 2013;**2013**:1-6. DOI: 10.1155/2013/760685

[34] Prajongtat P, Suramitr S, Nokbin S, Nakajima K, Misuke K, Hannongbua S. Density functional theory study of adsorption geometries and electronic structures of azo-based molecules on anatase TiO_2 surface for dye-sensitized solar cell applications. Journal of Molecular Graphics and Modelling. 2017; **76**:551-561. DOI: 10.1016/j.jmgm.2017.06.002

[35] Barbara V, Folarin W, Thomas B, Dominic L. Dye bonding to TiO_2: In situ attenuated Total reflection infrared spectroscopy study, simulations and correlation with dye sensitized solar cell characteristics. ACS Publications, American Chemical Society. 2012;**28**:11354-11363. DOI: 10.1021/la302197z

[36] Chiara A, Edoardo M, Mariachiara P, Enrico R, Fillipo De A. Adsorption of organic dyes on TiO_2 surfaces in dye-sensitized solar cells: Interplay of theory and experiment. Physical Chemistry Chemical Physics. 2012;**14**:15963-15974. DOI: 10.1039/C2CP43006A

[37] Jun Z, Lisha Q, Wei F, Junhua X, Zhenguo J. Alkaline- earth metal Ca and N codoped with TiO_2 with exposed (001) facets for enhancing visible light photocatalytic activity. American Ceramic Society**.** 2014;**97**:2615-2622. DOI: 10.1111/jace.12957

[38] Wenhui X, Xingo M, Tong W, Zhigi H, Wang H, Huang C. First-principles study on the synergistic effects of codoped TiO_2 photocatalysts codoped with N/V or C/Cr. Journal of Semiconductors. 2014;**35**:1-7. DOI: 10.1088/1674-4926/35/10/102002

[39] Puyad AL, Kumar CR, Bhanuprakash K. Adsorption of croconate dyes on TiO_2 anatase (101) surface: A periodic DFT study to understand the binding of diketone groups. Journal of Chemical Sciences. 2012;**124**:301-310. DOI: 10.1007/s12039-012-0229-1

[40] Chitumalla RK, Manho L, Xingfa G, Joonkyung J. Substituent effects on the croconate dyes in dye sensitized solar cell applications: A density functional theory study. Journal of Molecular Model. 2015;**21**:1-8. DOI: 10.1007/s00894-015-2845-4

[41] Leonardo T, Ana B, Munoz-G, Angela A, Michele P. First principles study of trimethylamine adsorption on anatase TiO_2 nanorod surfaces. Theoretical Chemistry Accounts. 2015;**134**:1-11. DOI: 10.1007/s00214-015-1721-8

[42] Elegbeleye IF, Maluta EN, Maphanga RR. Density functional theory

studies of ruthenium dye (N3) adsorbed on a TiO_2 Brookite cluster for application in dye sensitized solar cells. Advances in Quantum Systems in Chemistry, Physics, and Biology, Progress in Theoretical Chemistry and Physics, Springer Nature. 2020;**32**:143-155. DOI: 10.1007/978-3-030-34941-7_8

[43] Clark SJ, Segall MD, Pickard CJ, Hasnip PJ, Probert MJ, Refson K, et al. First principle methods using CASTEP. Zeithchrift fuer Kristallographie. 2005;**220**(5–6):576-570. DOI: 10.1524/zkri.220.5.567.65075

[44] Mortensen JJ, Hansen LB, Jacobsen KW. Real space grid implementation of the projector augumented wave method (GPAW). Physical Review B. 2005;**71**:1-11. DOI: 10.1103/PhysRevB.71.035109